Chemical Engineering Journal 215–216 (2013) 969–978

Contents lists available at SciVerse ScienceDirect

Chemical Engineering Journal

journal homepage: www.elsevier.com/locate/cej

Degradation of organic dye by pulsed discharge non-thermal plasma technology assisted with modified activated carbon fibers

Bo Jiang, Jingtang Zheng *, Xiu Lu, Qian Liu, Mingbo Wu *, Zifeng Yan, Shi Qiu, Qingzhong Xue, Zhenxing Wei, Huiji Xiao, Mengmeng Liu

State Key Laboratory of Heavy Oil Processing, China University of Petroleum, Qingdao 266555, Shandong, PR China

HIGHLIGHTS

- Combined systems of plasma and modified ACF samples were utilized for MO removal.
- The adsorption–catalytic effects of ACFs with various modification methods were studied.
- The property changes of MO solution were estimated in various degradation processes.
- Plasma degradation, adsorption and synergistic effect for organic removal were extensively evaluated.

GRAPHICAL ABSTRACT

Plasma degradation, adsorption and synergistic effect for organic removal were extensively studied and synergistic effect played an important role for organic removal in combined degradation processes.

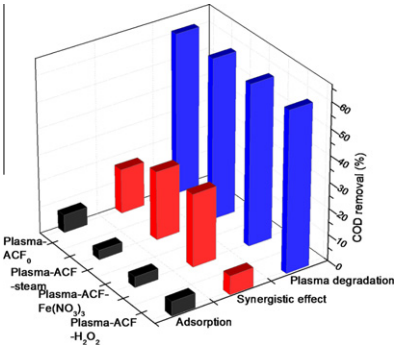

ARTICLE INFO

Article history:
Received 22 July 2012
Received in revised form 10 October 2012
Accepted 9 November 2012
Available online 17 November 2012

Keywords:
Activated carbon fiber
Surface modification
Methyl orange
Non-thermal plasma

ABSTRACT

Methyl orange (MO) was employed to evaluate degradation efficiency of the synergistic effect of activated carbon fibers (ACFs) and pulsed discharge non-thermal plasma in aqueous solution. In order to study the roles of the ACFs during the degradation activities, adsorption–catalytic effects of ACF samples modified with H_2O_2, $Fe(NO_3)_3$ and steam were assessed. The chemical and physical properties of these ACFs were characterized by XRD, SEM, BET and chemical titration methods. For comparative purposes, experiments of adsorption on ACF samples, plasma degradation, and plasma degradation in the presence of ACF samples were carried out. Plasma alone can obtain the decoloration of 77.3% for 100 mg/L MO solution and generate H_2O_2 (0.88 mM) and O_3 (0.025 mM) after 30 min treatment. Results also showed that the presence of either ACF_0 or modified ACFs considerably improved MO decoloration and COD removal in the plasma reactor. Compared with ACF_0 and ACF–H_2O_2, a total decoloration of MO and above 90% COD removal were obtained in approximately 30 min for ACF–steam and ACF–$Fe(NO_3)_3$ due to their larger adsorption capacities and better catalytic effects. In combined degradation processes, the yields of H_2O_2 and O_3 all decreased in presence of ACF samples as compared with plasma alone process. It was also observed that ACF samples can be well regenerated in combined processes and their adsorption behaviors contributed little for final organic removal.

1. Introduction

Dyes and pigments are widely used in various industries to color the final products and 10–15% of the world's total output of dye

* Corresponding authors. Tel.: +86 13854628317; fax: +86 546 8395190 (J. Zheng), tel.: +86 13505468246; fax: +86 86983452 (M. Wu).
E-mail addresses: jtzheng03@163.com (J. Zheng), wmbpeter@yahoo.com (M. Wu).

1385-8947/$ - see front matter © 2012 Elsevier B.V. All rights reserved.
http://dx.doi.org/10.1016/j.cej.2012.11.046

products are released directly into the environment as wastewater. These dyes are toxic, biologically rather resistant and apt to cause genetic mutations, and thus have to be removed before discharging into aquatic ecosystems [1,2].

Various traditional treatments for dye wastewater remediation such as biological treatment [3], ultrafiltration [4,5], adsorption [6,7] and coagulation–flocculation [8] have been reported in recent decades. Among these treatments, adsorption is a conventional but effective process by which the substance is transferred from the liquid phase to the surface of the solid and becomes bound by physical and/or chemical interactions at ambient environment [9]. Due to their excellent adsorption properties, large porous volumes and vast surface areas, porous carbon materials (e.g. activated carbons, carbon nanotubes, ordered mesoporous carbons, etc.) have been widely used as adsorbents for wastewater treatment [9–12]. For example, Altenor et al. [11] prepared vetiver roots-based activated carbon with high surface area (>1000 m^2/g) and high pore volume (up to 1.19 cm^3/g) and applied this material for methylene blue removal. It was found that methylene blue was favourably adsorbed by the large micropores or mesopores of vetiver roots-based activated carbon prepared by phosphoric acid activation. Although, activated carbons (AC) can efficiently remove dye molecules from liquid phase, it is energy consuming and complicated to regenerate these absorbents [13]. Thus, the need for environmentally friendly technologies, which would not result in the creation of more hazardous by-products, has led to an increased interest in the application of advanced oxidation processes (AOPs), including photocatalytic oxidation [14], ultrasound [15], Fenton processes [16], UV/H_2O_2 [17,18], UV/Fenton [19], etc. The Fenton reaction needs metal ions additions which catalytically decompose the hydrogen peroxide into hydroxyl radicals. UV light generated by a Xe lamp of hundreds of Watt or higher has great degradation efficiency of organic only when being combined with some chemical additions such as TiO_2, H_2O_2 and Fe^{2+}. Unfortunately, these technologies are high energy consumption and environmentally hazardous. As compared to other common AOPs, the non-thermal plasma technology has the capability to directly generate oxidizing species: radicals (e.g. ·H, ·O, ·OH, etc.), molecules (e.g. H_2O_2, O_3, etc.) and physical effects including weak-to-moderate UV light, shock waves, cavitation, etc. [20,21]. In plasma treatment processes, with an oxidation potential of 2.8 V, hydroxyl radical oxidations may be primary for organic degradation. While other oxidizing products (e.g. H_2O_2, O_3, etc.) do not only consume energy but also are not powerful enough to degrade recalcitrant compounds due to their relatively low oxidation potential. Thus, H_2O_2 and O_3 generated require to be activated with catalysts to produce higher active species which in turn enhance their oxidizing capability.

A number of studies reported that AC could give rise to the possibility of catalytic oxidation reactions on the surface of ACF in the oxidizing environment [22–24]. Kurniawan et al. [24] investigated the treatment performance of H_2O_2 oxidation alone and its combination with granular activated carbon adsorption for raw leachate with an initial COD concentration of 8000 mg/L and NH_3–N of 2595 mg/L. It was reasonably accepted in the literature that combination processes exhibited better pollutant removal (COD: 82%; NH_3–N: 59%) than H_2O_2 alone (COD: 33%; NH_3–N: 4.9%) and AC adsorption (COD: 58%) due to the adsorption–catalytic effect of AC. In ozonation alone process, ozone has been proved capable of degrading organic compounds in aqueous solution. However, ozonation processes generally suffer from restrictions due to interphase mass transfer resistance and consequently only partial oxidations of refractory organic compounds occur in aqueous solution [25,26]. Therefore, the application of ozonation might not be feasible from an economic point of view. Jans and Hoigné [27] published an excellent work on the aqueous ozone decomposition in the presence of AC. They observed an increase in the rate of ozone decomposition when AC was present and draw the conclusion that hydroxyl radicals were produced as a consequence of ozone–carbon interactions. Thus, combination of AC and ozonation into a single process can effectively enhanced the ozonation efficiency for organic removal and widely utilized for purifying food-processing wastewater [28], leachate from the landfill [29], and dye wastewater [30], etc.

In this regard, an integrated treatment process with non-thermal plasma technology and sorbent–catalyst materials like AC can offer an attractive alternative for wastewater remediation, as the two treatments may synergize the advantages of their treatment performances, while overcoming their respective limitations.

Previous works [31,32] have shown that the combination of pulsed discharge and AC has a synergistic effect on the degradation of phenol and parachlorophenol from solution. As a novel porous carbon, the advantages of ACF are the smaller fiber diameter, which minimizes diffusion limitations, more concentrated micropore size distribution and faster adsorption/desorption rate owing to numerous pores directly exposing on the surface as compared to conventional granular/powder activated carbons [33,34]. Moreover, another important advantage of ACFs is that they can be fabricated in different physical forms and hence easily recycled when acting as adsorbent and catalyst support [35]. Based on current knowledge about ACFs, more advantages may be visualized by combining ACF with plasma for wastewater treatment.

In current study, the objectives were examination of degradation efficiency of the combined systems of plasma and modified ACF samples, focusing on the adsorption–catalytic effects of ACF samples with various modification methods in plasma reactor. MO was selected as a model contaminant in this study due to its complex structure, high resistance to biodegradation and relatively high toxicity.

2. Materials and methods

2.1. Materials and apparatus system

Commercial viscose-based ACF felt was cut into 3 mm × 3 mm pieces, rinsed with distilled water, and dried at 383 K for 6 h. This material was designated ACF_0. All chemicals were provided from Sinopharm Chemical Reagent Co., Ltd. and used as received without further purification. The experimental apparatus was made up of a pulse power supply and a non-equilibrium plasma-based water treatment reactor, as illustrated in Fig. 1. The reactor was a 400 mL glass vessel and mainly consisted of high voltage pin-electrodes, ground electrode and sampling pipe. Compressed oxygen gas was bubbled into the discharge zone through a gas flow-meter and air inlet tube with a flow rate of 0.08 m^3/h. High voltage was applied to the high voltage electrode set in a perforated resin plate at the bottom of the reactor. The ground electrode suspended in gas phase with the distance of 15 mm above the high-voltage electrode. As electric discharge occurred in the reactor system, active species such as hydroxyl radical and hydrogen peroxide were produced in the liquid phase, while ozone was generated in the gas phase. Meanwhile, ozone rose and reacted with organic pollutant in reservoir, thus a pre-oxidation zone was formed.

2.2. Experimental methods and analysis

ACF–H_2O_2 and ACF–$Fe(NO_3)_3$ were prepared by wetness impregnation methods. Two equal portions of ACF_0 sample (3 g) were separately impregnated into two flasks containing H_2O_2 solution (200 mL, 6.53 M) for 3 h and $Fe(NO_3)_3$ solution (200 mL, 0.15 M) for 1 h. After impregnations, the former ACF samples were rinsed with distilled water and dried at 105 °C for 24 h. And the

latter was dried for 6 h at the temperature of 100 °C, which was followed by calcining at 345 °C for 30 min. For physical modification, ACF_0 was modified by steam at the temperature of 850 °C and the corresponding modified sample was labeled as ACF–steam.

Nitrogen adsorption isotherms were obtained by using BET surface area apparatus (Micromeritics, model ASAP 2000) at 77 K. The surface morphologies of ACFs were studied using a field-emission scanning electron microscope (KYKY-2800B). X-ray diffraction (XRD) patterns were obtained using a Holland X'pert PRO MRD diffractometer with Cu Ka radiation. The chemical titration method [36] was used in order to calculate the surface functionalities of each modified ACFs. The point of zero charge (pH_{PZC}) was measured by the mass titration/pH equilibration method [37].

In experiments, the reactor was filled with 200 mL MO solution, either with or without 0.35 g ACF for 30 min treatment. Adsorption experiments were also conducted in this reactor with the same condition in absence of electrical discharge. All degradation experiments were conducted with a fixed applied voltage of 40 kV, pulse repetition frequency of 100 pulses per second (pps), and charging capacitance of 67 pF. The corresponding pulse energy was 6.17 mJ and average power was 5.36 W. Typically, 3 mL samples were taken from the reactor vessel at fixed intervals during each run.

The concentrations of MO solution were calculated by measuring the absorbencies of the solution at 465 nm wavelength using Hach DR-2500 Spectrophotometer. The chemical oxygen demand (COD) was measured with a CM-02 COD analyzer (Beijing Shuanghui Corp., China). The concentrations of hydrogen peroxide and ozone were determined spectrophotometrically using Hach DR-2500 Spectrophotometer [38,39]. The absolute synergetic effect of combined processes is the removal difference between experimental and theoretical conversions, the latter is defined as the algebraic sum of plasma alone and adsorption contribution for final MO removal in the combined process.

MO removal rates could be described by first-order kinetics with good correlation coefficient values (>0.96):

$$\mathrm{Ln}\left(\frac{C}{C_0}\right) = -kt \tag{1}$$

The COD removal was calculated using the following equation:

$$\mathrm{COD}\ (\%) = \frac{\mathrm{COD}_0 - \mathrm{COD}}{\mathrm{COD}_0} \times 100 \tag{2}$$

where COD_0 is the chemical oxygen demand of initial solution and COD is the chemical oxygen demand at time t (min).

The $G_{37\%}$ presents the energy efficiency of degradation process when the concentration of target reduced to 37% of its initial concentration and can be estimated based on first order kinetics as below:

$$G_{37\%}\ (\mathrm{mg/J}) = \frac{0.63C_0V}{Pt_{37}} = \frac{0.63kC_0V}{P} \tag{3}$$

C_0 (mg/L) is the initial concentration of MO, respectively. V (L) is total solution volume. And P (W) is input power.

3. Results and discussion

3.1. Characterization of the ACF sample

The nitrogen adsorption isotherm of these two ACF samples are shown in Fig. 2a and the surface physical properties of the ACFs are summarized in Table 1. Hydrogen peroxide oxidation brought about an increase in surface area, pore volume and average pore diameter of ACF, as well as a large increase in the number of acidic groups, which resulted in a decrease in pH_{PZC}. It can be assigned to that H_2O_2 oxidation led to the etching of ACF surface and the formation of acidic oxygen groups or structures such as —C=O,—CO_2^- and —OH [40,41]. After ferric salt treatment, ACF samples expressed no significant change in surface physical properties, but the number of basic groups and acidic groups both reduced, which resulted in a slight increase in pH_{PZC}. This may be a result of decompositions of partial acidic and basic groups when ferric nitrate was thermally decomposed on the surface of ACF. Table 1 illustrates that steam gave rise to an obvious increment of BET area and pore volume. The pore size distribution in Fig. 2b shows that there are the two main peaks and some minor peaks of ACF–steam within the range of micropore diameters (0–2 nm), which suggested that larger micropore volume can be created by steam modifying. And according to Table 1, no obvious change of surface chemical properties was detected after steam modifying.

The X-ray diffraction patterns of selected catalysts are presented in Fig. 3. It is obvious that ACF–H_2O_2 and ACF–steam had similar peaks with ACF_0. The characteristic reflections at $2\theta = 33.0°$, 35.5° and 40.78° correspond to α-Fe_2O_3. Thus, metal oxide successfully dispersed on the surface of the support.

Fig. 4 depicts the surface morphology of ACF samples. It is observed that there were many long axial grooves on the surface of original ACF and the surface was relatively smoothly. After H_2O_2 modification, although axial fiber structure was reserved, there were many crackings appearing on the ACF surface, the skin layer

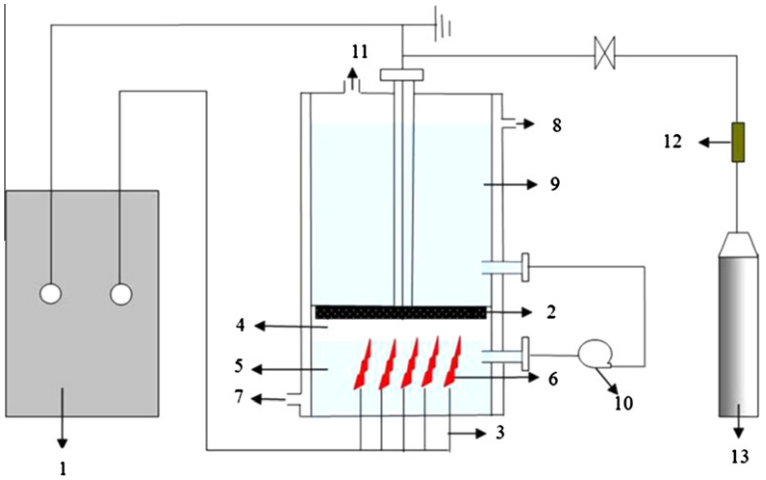

Fig. 1. Reactor configuration: 1. Pulse power supply; 2. Earthed electrode; 3. High voltage pin-electrodes; 4. Gas discharge zone; 5. Liquid discharge zone; 6. Discharge streamer; 7. Cooling water inlet; 8. Cooling water outlet; 9. Pretreatment wastewater; 10. Peristaltic pump; 11. Sampling pipe; 12. Flowmeter; 13. Oxygen container.

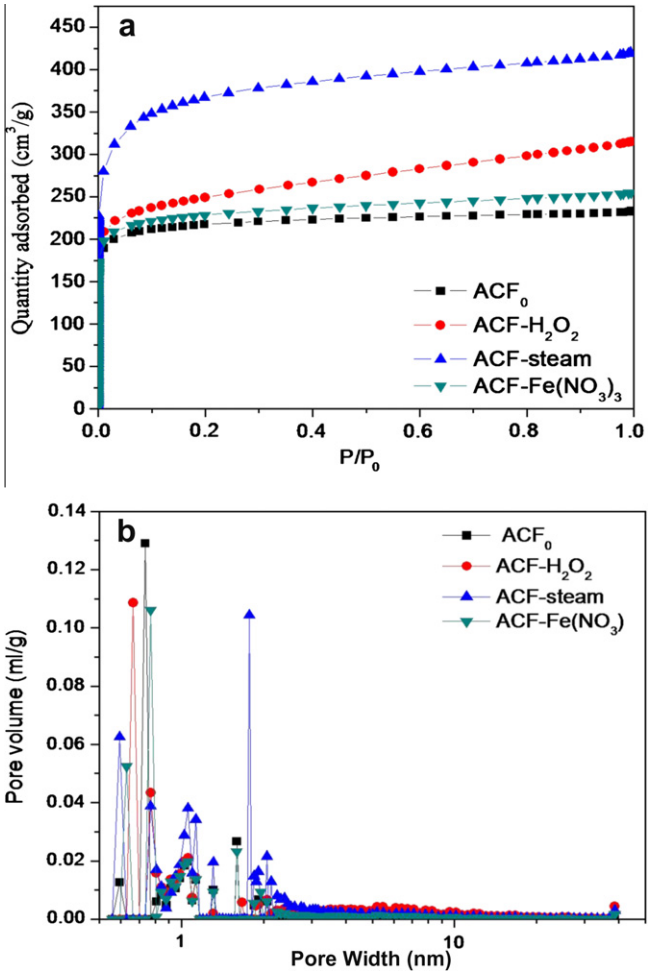

Fig. 2. (a) Nitrogen adsorption isotherms and (b) corresponding pore diameters distribution obtained by the DFT of ACF_0, ACF–H_2O_2, ACF–steam and ACF–$Fe(NO_3)_3$.

was likely peeling off, and the surface was rather rough. While, surface morphology of ACF–steam had no distinct change in comparison with ACF_0 indicating ACF surface was not destroyed after steam modifying. Fig. 4d shows that nanostructured irons were successfully loaded on ACF and structure of ACF samples were well retained.

3.2. Degradation activity

3.2.1. MO decoloration in plasma alone process

In this study, the applied apparatus was a circulating gas–liquid hybrid discharge non-thermal plasma reactor. The advantage of hybrid reactor was ozone generation in gas phase, as well as producing short- and long-term oxidative species (·OH, ·O_2H, H_2O_2, etc.) in discharge zones [20,21]. This can be partially verified by the result that the concentrations of hydrogen peroxide and dissolved ozone in aqueous solution were 0.88 mM and 0.025 mM. The decoloration efficiency is shown in Fig. 5, non-thermal plasma can relatively efficiently decompose the chromophore groups of dye molecules and the decoloration efficiency decreased with increase of initial solution concentration. For example, after 30 min plasma treatment, the decoloration efficiency was 87.7% for 40 mg/L and reduced to 77.3% for 100 mg/L.

3.2.2. MO decoloration in combined process

The decoloration curves of 60 mg/L MO aqueous solution are portrayed in Fig. 6. It can be observed that the MO decoloration efficiency increased in the presence of ACF samples in plasma reactor, especially for ACF–steam and ACF–$Fe(NO_3)_3$. The MO decoloration efficiency was capable of quick achieving 96.5% after 30 min treatment with introducing ACF_0 into plasma reactor. Table 2 shows that compared with plasma alone, $G_{37\%}$ and rate constant for plasma–ACF_0 both enhanced 58%. We know ACF_0 naturally owned numerous O-content functional groups, basic catalytic sites as well as relative large surface area and pore volume. And it is confirmed that chemical features of AC can provoke decomposition of ozone and hydrogen peroxide into HO·, which favored destruction of organic.

In Fig. 6 and Table 2, we observe that plasma–ACF–steam displayed largest decoloration efficiency and fastest decoloration rate in 30 min treatment process. Approximately 96% of MO was degraded after 15 min treatment. According to many publications, ozone and hydrogen peroxide decompositions in the presence of AC are dependent on both chemical and textural features of AC surface [42]. And it has been accepted that heterogeneous ozone decomposition is enhanced by AC with high surface area and large basicity. From Table 1, in the process of steam activating ACF samples at the temperature of 850 °C, more micropores and mesopores were created on the surface of ACF indicating high adsorption capacity for organic contaminant, which favored the decomposition of ozone and hydrogen peroxide and generation of highly active species. Thus, although ACF–steam had similar chemical properties with that of ACF_0, $G_{37\%}$ and rate constant for plasma–ACF–steam increased 67.8% in comparison with plasma–ACF_0.

The classical homogeneous Fenton system has been extensively studied for the oxidation of a great variety of organic contaminants in water [43]. Iron ions in solution for homogeneous Fenton reaction are very hard to separate and recover hindering the application of homogeneous reaction. To overcome these disadvantages, heterogeneous catalysts supporting ferric ions have been developed which can operate at near neutral pH and draw considerable interest since they could offer some advantages, such as no need of acid or base, no sludge generation and the possibility of recycling the catalyst [44–46]. In these degradation processes, electrical discharge plasma produced oxidizing environment containing H_2O_2, O_3 and other species in reactor, which was desirable condition for Fenton reaction. Table 1 shows that ACF–$Fe(NO_3)_3$ had a reduction in basic groups and similar physical surface property with ACF_0. However, it is worth noting that ACF–$Fe(NO_3)_3$ had higher capacity for MO removal. It is possible that the iron oxides formed, highly dispersed on the carbon surface was active for H_2O_2 decomposition into ·OH suggesting the acceleration of degrading MO into harmless product.

The related equations are summarized as follows [45,46]:

$$\equiv Fe^{2+} \cdot H_2O + H_2O_2 \rightarrow \equiv Fe^{2+} \cdot H_2O_2 \rightarrow \equiv Fe^{3+} + \cdot OH + OH^- \quad (4)$$

$$\equiv Fe^{3+} + H_2O_2 \rightarrow \equiv Fe^{3+} \cdot H_2O_2 \rightarrow \equiv Fe^{2+} + \cdot OOH + H^+ \quad (5)$$

Table 1
Textural characteristics of ACF samples.

ACF	S_{BET} (cm^2/g)	S_{mi} (m^2/g)	V_{mic} (cm^3/g)	V_t (cm^3/g)	Wp (A)	Acidic groups (mmol g^{-1})	Basic groups (mmol g^{-1})	pH_{PZC}
ACF_0	736	620	0.30	0.36	1.96	3.42	0.55	6.76
ACF–H_2O_2	849	587	0.33	0.49	2.30	6.20	0.17	5.03
ACF–steam	1259	847	0.39	0.65	2.06	3.26	0.57	6.81
ACF–$Fe(NO_3)_3$	774	638	0.29	0.39	2.04	1.67	0.39	6.98

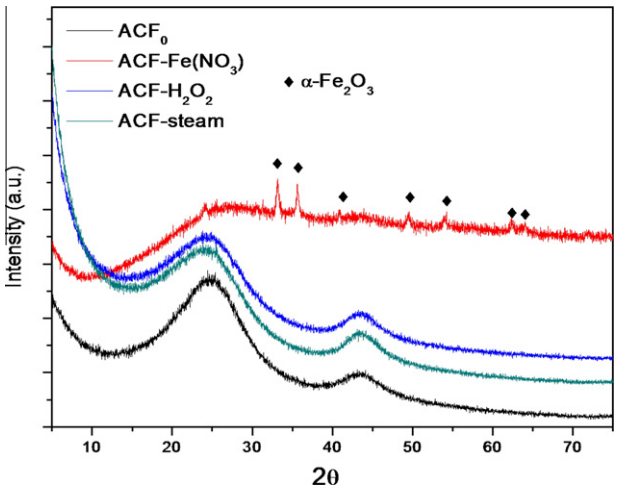

Fig. 3. The X-ray powder diffraction patterns of ACFs.

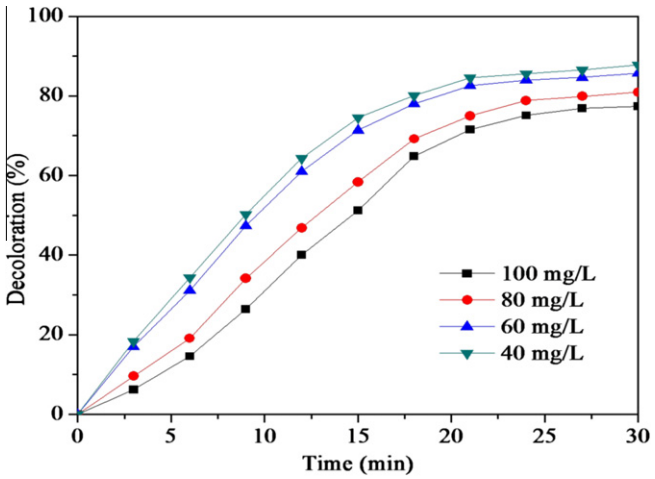

Fig. 5. MO removal percentage as a function of treatment time with different initial concentration (conditions: input energy 5.36 W; total volume 200 mL; treatment time 30 min; ambient condition).

$$\equiv Fe^{3+} + {}^{\cdot}OOH \rightarrow \equiv Fe^{2+} + O_2 + H^+ \quad (6)$$

While, it is interestingly noted that, compared with that of ACF_0, worse adsorption–catalytic effect for ACF–H_2O_2 was deduced from slower decoloration rate and less decoloration efficiency in Table 2. It can be attributed to that, as shown in Table 1, H_2O_2 oxidation reduced the number of basic groups and consequently catalytic effect of this sample had obvious decrease.

Above, these coupled plasma degradation processes with suitable ACF have the potential for wastewater remediation. Thus far, a large variety of electrochemical advanced oxidation processes have also been developed, such as gliding arc discharge [47] and contact glow discharge electrolysis [48]. In Table 2, though being greatly improved using the Fenton's reagent or photocatalyst, the energy efficiencies of these technologies were 2 orders of magnitude lower in comparison with pulsed electrical discharge plasma technology. As regards many other AOPs, lots of achievements have been gotten about their application in bench scale. However, take UV-based processes as an example, majority of UV lights cannot efficiently captured by catalyst leading to relatively low energy efficiency as shown in Table 2.

3.2.3. COD removal

The results corresponding to COD removal after 30 min are presented in Fig. 7. This is an indication that plasma by itself can decompose the organic groups of the dye molecules and also originated a decrease in the value of COD (61.5% removal) in solution. In Fig. 6, rapid decolorations were observed after 30 min when combined processes of plasma–ACFs were applied. Nevertheless, the mineralization levels were much lower than color removal as presented in Fig. 7, which suggested that part of the dye degradation products (colorless) remained in solution. In all cases, the decrease

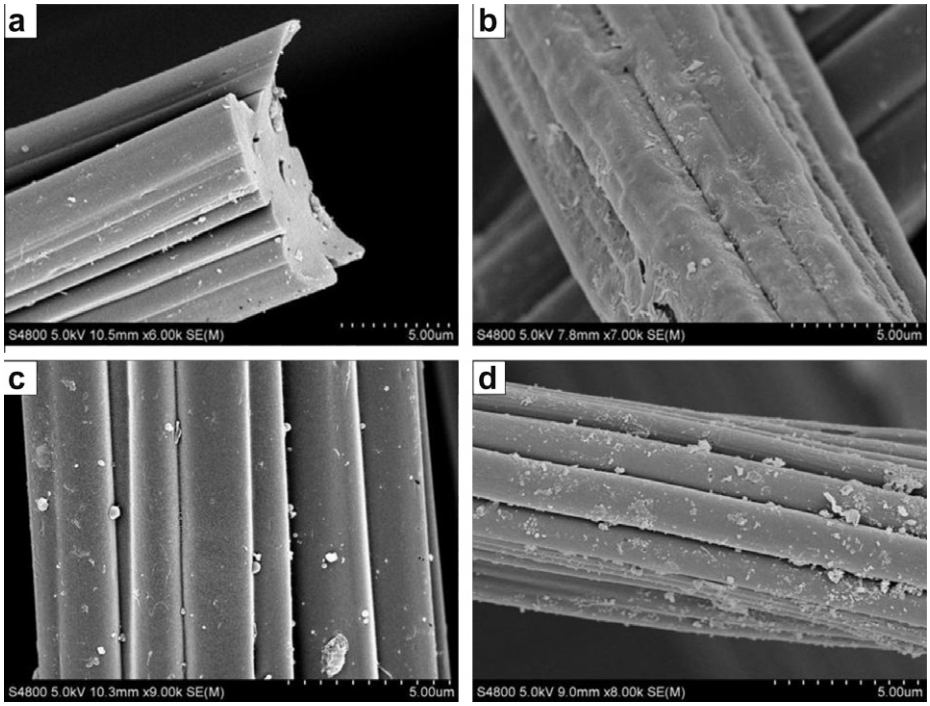

Fig. 4. SEM images of ACF_0 and modified ACF samples: (a) ACF_0, (b) ACF–H_2O_2, (c) ACF–steam and (d) ACF–$Fe(NO_3)_3$.

in COD concentration followed the same trend as decoloration efficiency: plasma < plasma–ACF–H_2O_2 < plasma–ACF_0 < plasma–ACF–$Fe(NO_3)_3$ < plasma–ACF–steam.

3.2.4. Concentrations of H_2O_2 and O_3 generated

In the reactor used in present study, the discharge electrodes were five acupuncture needles which were inserted at the bottom of reactor through which gas was supplied into the discharge region, forming gas bubbles surrounding needle tips. As the discharge occurred, the gas and water molecules in the discharge region were dissociated or excited to form hybrid phase plasma, which was responsible for the generation of O_3 and H_2O_2 in reactor.

Related reactions describing the generation of O_3 and H_2O_2 are exhibited as follows [20,21,49]:

$$e^- + O_2 \rightarrow O + O + e^- \quad (7)$$

$$O + O_2 \rightarrow O_3 \quad (8)$$

$$e^- + O_2 \rightarrow O_2^* + e^- \quad (9)$$

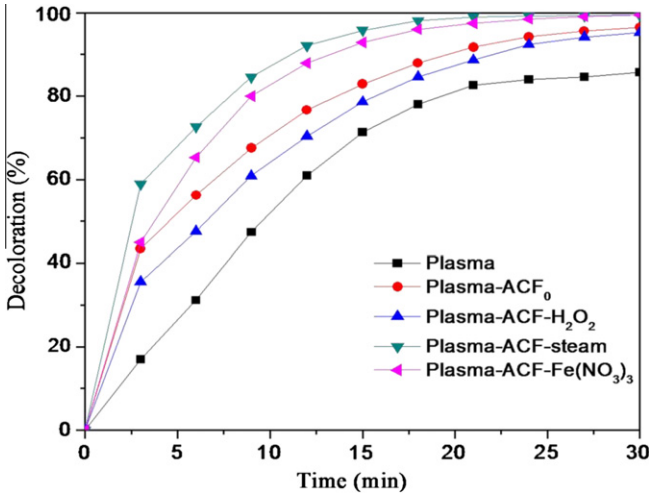

Fig. 6. MO removal percentage as a function of treatment time with different ACF simples (conditions: input energy 5.36 W; total volume 200 mL; initial concentration 60 mg/L; treatment time 30 min; ACF 0.35 g; ambient condition).

$$O_2^* + O_2 \rightarrow O_3 + O \quad (10)$$

$$e^- + O_3 \rightarrow O + O_2 + e^- \quad (11)$$

$$\cdot OH + O_3 \rightarrow \cdot O_2H + O_2 \quad (12)$$

$$\cdot O_2H + O_3 \rightarrow \cdot OH + 2O_2 \quad (13)$$

$$e^- + H_2O \rightarrow \cdot OH + \cdot H \quad (14)$$

$$\cdot OH + \cdot OH \rightarrow H_2O_2 \quad (15)$$

$$O + H_2O \rightarrow \cdot OH + \cdot OH \quad (16)$$

$$H_2O_2 + \cdot OH \rightarrow H_2O + \cdot O_2H \quad (17)$$

Fig. 8 presents that compared with those in plasma alone process, the yields of O_3 and H_2O_2 significantly reduced after 30 min in combined treatment processes. It can be assigned to that some O_3 and H_2O_2 produced were catalytically decomposed into other species when adding various ACF samples in plasma reactor. As portrayed in Fig. 8 and shown in Table 1, it is interesting to note that the concentrations of O_3 in presence of ACF–$Fe(NO_3)_3$ and ACF–steam were similar even though the concentration of basic sites and the textural properties were very different. In combined process, the reaction system was very complex and consisted of the generations of active species (O_3, H_2O_2 and some radicals), heterogeneous Fenton reaction and adsorption–diffusion processes on the surface of ACF, etc. These actions interacted with each other and behaved synergistically according to reactions 4–17. For example, O_3 or its products may directly or indirectly take part in the generation and consumption of H_2O_2 and Fenton reaction. Thus, though ACF–$Fe(NO_3)_3$ had less catalytic ozonation effect in comparison with ACF–steam, the consumption of O_3 was expected as usual in this combined process.

3.2.5. The variation of solution pH during MO decoloration process

In plasma alone process, the general behavior of pH decreased as described in Fig. 9 and it can be attributed to acidic intermediates produced during the oxidation reaction which was in agreement with the presence of organic acids as stable products [50]. When adding ACF–steam in plasma degradation process, the decoloration rate of MO was catalytically enhanced and more acidic organics were produced. Consequently, compared with plasma alone process, pH of solution decreased faster from 6.2 to 3.9. After

Table 2
Rate constants and energy efficiencies of various degradation processes for dye removal.

Technology	Experiment conditions	Rate constant (min^{-1})	$G_{37\%}$ (10^{-3} mg/J)	Refs.
Pulsed electrical discharge plasma	*P*: 5.36; *C*: 60; *V*: 200; *T*: 30; Ta: methyl orange	0.074	1.74	This paper
Pulsed electrical discharge plasma	*P*: 5.36; *C*: 60; *V*: 200; *T*: 30; Ta: methyl orange; ACF_0: 0.35 g	0.117	2.75	This paper
Pulsed electrical discharge plasma	*P*: 5.36; *C*: 60; *V*: 200; *T*: 30; Ta: methyl orange; ACF–H_2O_2: 0.35 g	0.104	2.45	This paper
Pulsed electrical discharge plasma	*P*: 5.36; *C*: 60; *V*: 200; *T*: 30; Ta: methyl orange; ACF–steam: 0.35 g	0.196	4.61	This paper
Pulsed electrical discharge plasma	*P*: 5.36; *C*: 60; *V*: 200; *T*: 30; Ta: methyl orange; ACF–$Fe(NO_3)_3$: 0.35 g	0.176	4.14	This paper
Photocatalytic oxidation	*P*: 11; *C*: 5; *V*: 80; *T*: 240; Ta: methyl orange; mesoporous-assembled TiO_2: 2 g/L	0.615	0.235	[14]
Ultrasound	*P*: 100; *C*: 1000; *V*: 100; *T*: 40; Ta: acid orange 7; AC/ Fe^0: 2.3 g	0.0391	0.041	[15]
UV/H_2O_2	*P*: 6; *C*: 25; *V*: 50; *T*: 10; Ta: remazol turquoise blue; H_2O_2: 12 mM	0.043	0.094	[17]
Photo-Fenton	*P*: 48; *C*: 50; *V*: 500; *T*: 90; Ta: Remazol Brilliant Orange 3R; Iron exchanged zeolite: 1 g/L; H_2O_2: 15 mM	0.0482	0.264	[19]
Gliding arc disch-arge	*P*: 100; *C*: 50; *V*: 180; *T*: 180; Ta: anthraquinonic acid green 25; TiO_2: 2 g/L	0.043	0.041	[47]
Contact glow disch-arge electrolysis	*P*: 38; *C*: 4.15; *V*: 200; *T*: 40; Ta: methyl orange; Fe^{2+}: 2 mM	0.063	0.014	[48]

P – power (W); *C* – concentration (mg/L); *V* – volume (ml); *T* – time (min); Ta – target.

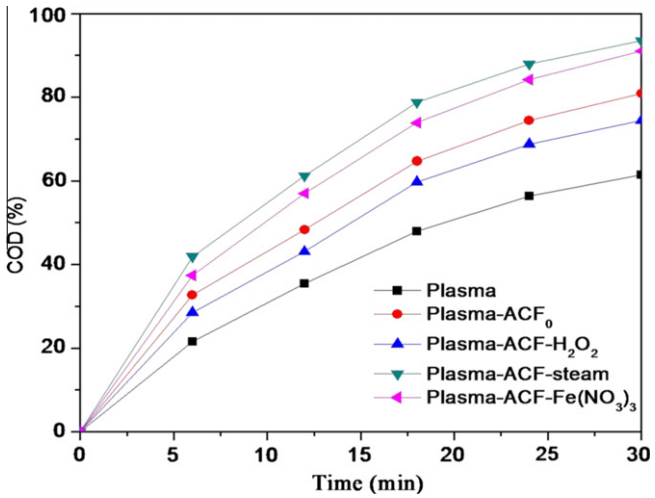

Fig. 7. COD removal percentage as a function of treatment time with different ACF simples (conditions: input energy 5.36 W; total volume 200 mL; initial concentration 60 mg/L; treatment time 30 min; ACF 0.35 g; ambient condition).

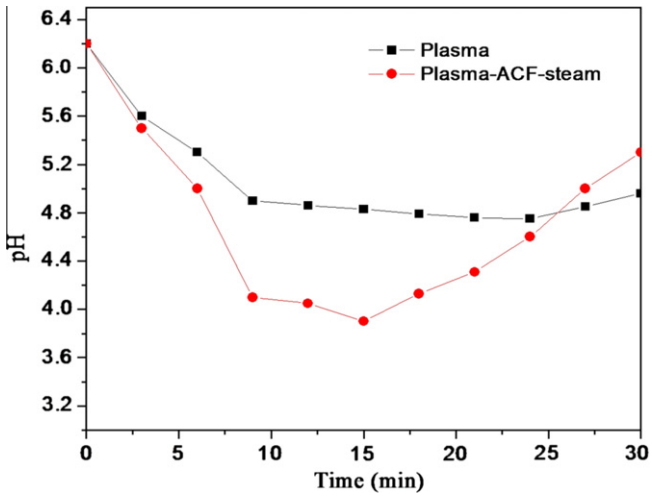

Fig. 9. The variation in pH during MO degradation (conditions: input energy 5.36 W; total volume 200 mL; initial concentration 60 mg/L; treatment time 30 min; ACF 0.35 g; ambient condition).

treatment time of 15 min, pH increased to 5.5 due to acidic intermediates being mineralized into CO_2 and H_2O.

3.3. Adsorption

When working with organic compounds removal, the adsorption capacity of the carbon samples towards these organic compounds plays a key role [22,26,51]. On one hand, adsorption competes with the oxidation reaction for the removal of pollutants from the aqueous phase. On the other hand, the adsorption step may greatly involve in the process of heterogeneous catalytic degradation. In this research, adsorption experiments were carried out to determine the adsorption characteristics of ACFs.

The pseudo-second-order model has been used as adsorption kinetic model in many studies and can be expressed as [52,53]:

$$\frac{t}{q_t} = \frac{1}{k_2 q_e^2} + \frac{t}{q_e} \tag{18}$$

where k_2 (g/(min mg)) is the second-order rate constant. The values of t/q_t are plotted against t, and q_e and k_2 are calculated from the slope and intercept of the plot.

The straight lines in Fig. 10 show a good agreement of experimental data with the second-order kinetic model for various ACF samples. Computed results obtained from the second-order kinetic model are listed in Table 3. It can be seen that the adsorption capacities and rate constants of ACFs followed the sequence: ACF–steam > ACF–Fe$(NO_3)_3$ > ACF$_0$ > ACF–H_2O_2. It is also found that adsorption capacities and rate constants of ACF samples have positive relationship with the decoloration efficiencies of corresponding combined processes. The degradation reactions on the surface of ACF samples were complex and mainly depended on the active species (H_2O_2 and O_3), catalytic effect of ACF and its absorption characteristic (adsorption capacity and adsorption rate). And it can be inferred that high adsorption capacity and fast adsorption rate favored the heterogeneous catalytic degradation and resulted in rapid decoloration rate in corresponding combined process.

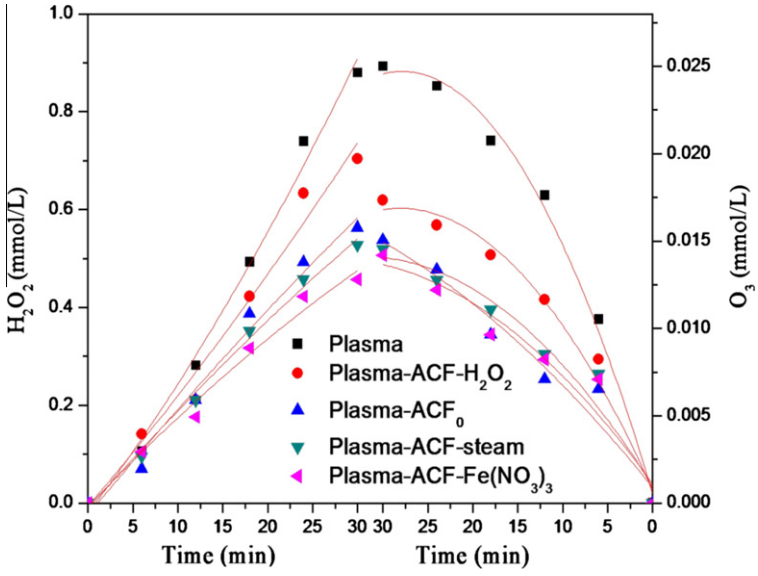

Fig. 8. Concentrations of H_2O_2 and O_3 as a function of time for different ACFs in MO solution (conditions: input energy 5.36 W; total volume 200 mL; initial concentration 60 mg/L; treatment time 30 min; ACF 0.35 g; ambient condition).

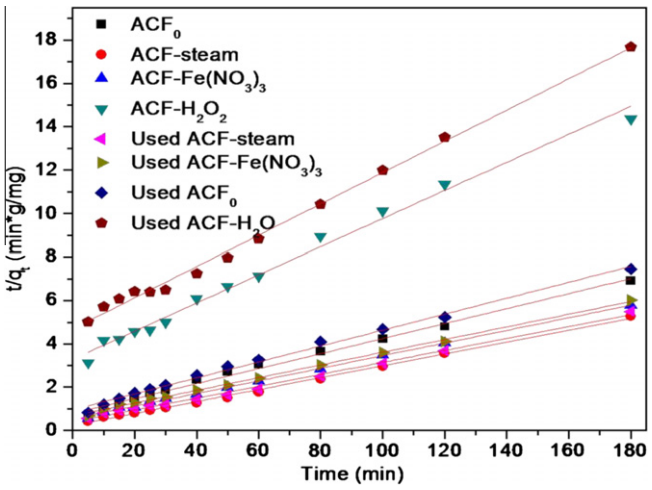

Fig. 10. Pseudo-second-order model fittings of the adsorption kinetics (conditions: total volume 200 mL; initial concentration 60 mg/L; treatment time 180 min; ACF 0.35 g; ambient condition).

Table 3
Pseudo-second-order constants for the adsorption of MO on ACFs.

ACF	Pseudo-second-order			
	Q_{180min}	k_2	q_e	R^2
ACF_0	26.05	0.00153	28.90	0.992
Used ACF_0	24.14	0.00141	27.20	0.994
ACF–H_2O_2	12.53	0.00128	15.44	0.990
Used ACF–H_2O_2	10.18	0.00111	13.87	0.995
ACF–steam	34.15	0.00314	36.42	0.998
Used ACF–steam	32.74	0.00188	36.42	0.995
ACF–$Fe(NO_3)_3$	31.14	0.00155	34.35	0.999
Used ACF–$Fe(NO_3)_3$	29.90	0.00125	34.15	0.998

For the adsorption process of ACF–$Fe(NO_3)_3$, equilibrium adsorption capacity for this ACF sample was 31.14 mg/g which was larger than 26.05 mg/g of ACF_0. It is proposed that the reduction in number of O-content groups may account for its adsorption capacity increase as compared to ACF_0. It is well known that the interactions of the molecules of dyes and the activated carbon surface is expected to occur between the delocalised π electrons of the oxygen-free Lewis basic sites and the free electrons of the dye molecule [52,54,55]. The oxygen-containing functional groups on AC surface, which are electron-withdrawing groups, reduce the electron density on the surface of the carbon and have a negative effect on the adsorption of anionic (acidic) species [56,57]. Therefore, lower adsorption capacity and slower adsorption rate were observed for ACF–H_2O_2 sample than those of other ACF samples. Moreover, an increase in acidic O-content groups of carbon produced by H_2O_2 oxidation diminished the basicity of the carbon surface (electronic density of the basal planes) and in turn reduced the pH_{pzc}. As a result, there was an increase in repulsive electrostatic interactions between the anions of the dyes and the negatively charged surface of ACF–H_2O_2 sample.

After being utilized in plasma systems, the adsorption capacities of ACF samples were also estimated. And all used samples have less adsorption capacity and slower adsorption rate than corresponding fresh samples. Take ACF–steam for example, MO removal decreased from 83.4% to 73.2% at 30 min and from 99.6% to 95.5% at 180 min. It is possible that some adsorption sites were occupied by some organic molecules in combined degradation process. From Fig. 11, it is worthy to observe that even when the individual contributions of the plasma degradation and adsorption were included, it presented 16.8, 27.9, 26 and 7.3% of absolute synergistic effect for ACF_0, ACF–steam, ACF–$Fe(NO_3)_3$ and ACF–H_2O_2, respectively. Besides, Fig. 11 shows that adsorption of ACF samples made little contribution for COD removal in plasma reactor where plasma degradation and the catalytic effect of ACF were primary for final COD removal.

3.4. Repeated use of ACF samples

In catalytic degradation processes, the investigation of catalyst stability in long-term reactions is of crucial importance for evaluating its applicability for wastewater treatment. Fig. 12 shows the COD removal of MO solution by five runs performed with used ACFs recovered by filtration and thoroughly dried in ambient temperature after each cycle. As can be seen, COD removal for ACF–steam was slightly dropped from 93.5% to 90.4% after five cycles.

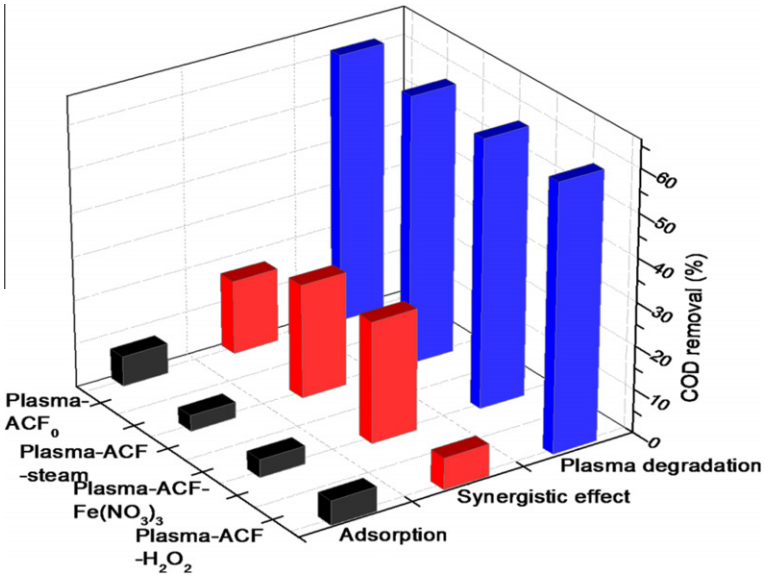

Fig. 11. The contributions of adsorption, plasma degradation and synergistic effect to the COD removal in the presence of ACF samples after 30 min of treatment.

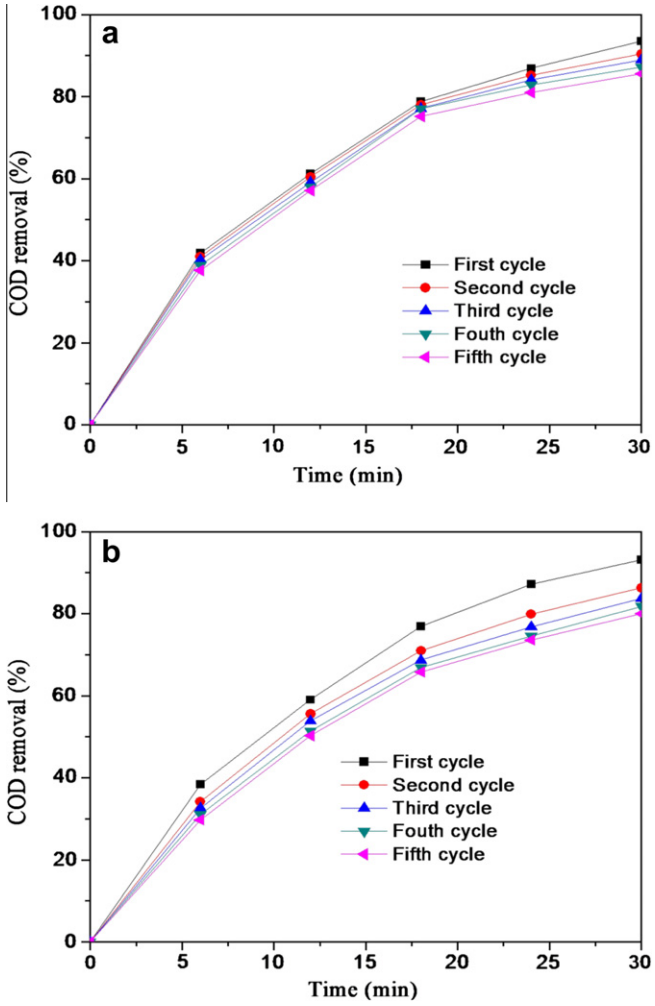

Fig. 12. Repeated use of ACF–steam (a) and ACF–Fe$(NO_3)_3$ (b) for COD removal in combined degradation processes (conditions: input energy 5.36 W; total volume 200 mL; initial concentration 60 mg/L; treatment time 30 min; ACF 0.35 g; ambient condition).

While, the efficiency for ACF–Fe$(NO_3)_3$ had distinct decrease, likely due to cumulative leaching of iron species from catalyst support in acidic solution [58].

3.5. The role of ACF samples during MO decoloration in plasma system

It is known that in the literature that H_2O_2 can be activated on the AC surface to generate hydroxyl free radicals [59]. The AC can be regarded to function as an electron-transfer catalyst just like the Haber–Weiss mechanism involving the reduced and oxidized catalyst states. When interacting with O_3 in aqueous solution, incorporated metal centers, electrons of the graphenic layers (basal plane electrons) and basic surface groups of AC can accelerate ozone decomposition resulting in the formation of hydroxyl radicals [26,60].

In combined processes, ACF samples provided a high surface area where both organic compounds and oxidizing molecules (O_3 and H_2O_2) can adsorb by physical or chemical effect. And then more ·OH were produced and attacked the accumulated organic into intermediates and finally into harmless products such as $H_2O, CO_2, NO_3^-, SO_4^{2-}$ [21]. Consequently, ACF samples can be timely regenerated. Above, The possible mechanisms of heterogeneous degradation is proposed in Eqs. (4)–(6) and (19)–(27) [24,32,51,52,61].

$$O_3 + H - ACF - H \rightarrow ACF - O + H_2O_2 \quad (19)$$

$$O_3 + ACF - OH \rightarrow \cdot O_2 - ACF + \cdot OH \quad (20)$$

$$O_3 - ACF \rightarrow O_2 + \cdot O - ACF \quad (21)$$

$$O_3 + \cdot O - ACF \rightarrow \cdot O_2 + O + ACF \quad (22)$$

$$ACFsurface) + H_2O_2 \rightarrow ACFsurface)^+ + OH^- + \cdot OH \quad (23)$$

$$ACFsurface)^+ + H_2O_2 \rightarrow ACFsurface) + H^+ + \cdot O_2H \quad (24)$$

$$ACFsurface) + MO \rightarrow ACFsurface) \cdots MO \quad (25)$$

$$ACFsurface) \cdots MO + \cdot OH \rightarrow ACFsurface) + Intermediates \quad (26)$$

$$\cdot OH + Intermediates \rightarrow CO_2 + H_2O \quad (27)$$

4. Summary

Coupled process of plasma and ACF can effectively remove MO in aqueous solution and is a promising technology for the treatment of refractory organic pollutants in view of fast removal rate and environmental friendliness. In this study, ACF samples with high adsorption capacity and preferable catalytic effect can significantly enhance the MO decoloration in combined processes. The COD removal for plasma–ACF–steam and ACF–Fe$(NO_3)_3$ was above 90% after 30 min treatment. Adding ACFs can reduced the concentrations of H_2O_2 and O_3 due to catalytic decompositions. In degradation processes, ACF samples can be well regenerated and sustain their adsorption capacities. After plasma treatment, little MO removal was ascribed for ACF adsorption. The indexes of rate constant and energy efficiency indicated the degradation enhancing effect of ACF in plasma reactor can maintained at a high level after repeated recycles.

Acknowledgments

This work is financially supported by National Natural Science Foundation of China (Nos. 20776159, 21176260, 51172285, 20876176) and Natural Science Foundation of Shandong province (No. 09CX05009A).

References

[1] L. Donnaperna, L. Duclaux, R. Gadiou, M.P. Hirn, C. Merli, L. Pietrelli, Comparison of adsorption of Remazol Black B and Acidol Red on microporous activated carbon felt, J. Colloid Interface Sci. 339 (2009) 275–284.
[2] C. Tizaoui, N. Grima, Adsorption of aromatic compounds by carbonaceous adsorbents: a comparative study on granular activated carbon, activated carbonfiber and carbon nanotubes, Environ. Sci. Technol. 44 (2010) 6377–6383.
[3] M. Kornaros, G. Lyberatos, Biological treatment of wastewaters from a dye manufacturing company using a trickling filter, J. Hazard. Mater. 136 (2006) 95–102.
[4] A.L. Ahmada, S.W. Puasab, M.M.D. Zulkali, Micellar-enhanced ultrafiltration for removal of reactive dyes from an aqueous solution, Desalination 191 (2006) 153–161.
[5] F. Banat, N.A. Bastaki, Treating dye wastewater by an integrated process of adsorption using activated carbon and ultrafiltration, Desalination 170 (2004) 69–75.
[6] E. Haque, J.W. Jun, S.H. Jhung, Adsorptive removal of methyl orange and methylene blue from aqueous solution with a metal-organic framework material, iron terephthalate (MOF-235), J. Hazard. Mater. 185 (2011) 507–511.
[7] K.P. Singh, D. Mohan, S. Sinha, Color removal from wastewater using low-cost activated carbon derived from agricultural waste material, Ind. Eng. Chem. Res. 42 (2003) 1965–1976.
[8] A. Szygu1a, E. Guibal, M.A. Palacın, Removal of an anionic dye (Acid Blue 92) by coagulation–flocculation using chitosan, J. Environ. Manage. 90 (2009) 2979–2986.

[9] L.R. Roberto, O.P. Raul, M.B. Jovita, External mass transfer and hindered diffusion of organic compounds in the adsorption on activated carbon cloth, Chem. Eng. J. 183 (2012) 141–151.
[10] X. Zhuang, Y. Wan, C.M. Feng, Y. Shen, D.Y. Zhao, Highly efficient adsorption of bulky dye molecules in wastewater on ordered mesoporous carbons, Chem. Mater. 21 (2009) 706–716.
[11] S. Altenor, B. Carene, E. Emmanuel, J. Lambert, J.J. Ehrhardt, S. Gaspard, Adsorption studies of methylene blue and phenol onto vetiver roots activated carbon prepared by chemical activation, J. Hazard. Mater. 165 (2009) 1029–1039.
[12] L.L. Ji, Y. Shao, Z.Y. Xu, S.R. Zheng, D.Q. Zhu, Adsorption of monoaromatic compounds and pharmaceutical antibiotics on carbon nanotubes activated by KOH etching, Environ. Sci. Technol. 44 (2010) 6429–6436.
[13] P.S. Yap, T.T. Lim, Solar regeneration of powdered activated carbon impregnated with visible-light responsive photocatalyst: factors affecting performances and predictive model, Water Res. 46 (2012) 3054–3064.
[14] P. Jantawasu, T. Sreethawong, S. Chavadej, Photocatalytic activity of nanocrystalline mesoporous-assembled TiO_2 photocatalyst for degradation of methyl orange monoazo dye in aqueous wastewater, Chem. Eng. J. 155 (2009) 223–233.
[15] H.N. Liu, G.T. Li, J.H. Qu, H.J. Liu, Degradation of azo dye Acid Orange 7 in water by Fe_0/granular activated carbon system in the presence of ultrasound, J. Hazard. Mater. 144 (2007) 180–186.
[16] M.S. Lucas, J.A. Peres, Decolorization of the azo dye Reactive Black 5 by Fenton and photo-Fenton oxidation, Dyes Pigm. 71 (2006) 236–244.
[17] Umme Kalsoom, S. Salman Ashraf, Mohammed A. Meetani, Degradation and kinetics of H_2O_2 assisted photochemical oxidation of Remazol Turquoise Blue, Chem. Eng. J. 200–202 (2012) 373–379.
[18] S. Haji, B. Benstaali, N.A. Bastaki, Degradation of methyl orange by UV/H_2O_2 advanced oxidation process, Chem. Eng. J. 168 (2011) 134–139.
[19] Mesut Tekbas, H. Cengiz Yatmaz, Nihal Bektas, Heterogeneous photo-Fenton oxidation of reactive azo dye solutions using iron exchanged zeolite as a catalyst, Micropor. Mesopor. Mater. 115 (2008) 594–602.
[20] B.R. Locke, M. Sato, P. Sunka, M.R. Hoffmann, J.S. Chang, Electrohydraulic discharge and nonthermal plasma for water treatment, Ind. Eng. Chem. Res. 45 (2006) 882–905.
[21] B. Jiang, J.T. Zheng, Q. Liu, M.B. Wu, Degradation of azo dye using non-thermal plasma advanced oxidation process in a circulatory airtight reactor system, Chem. Eng. J. 204–206 (2012) 32–39.
[22] P.C.C. Faria, J.J.M. Órfão, M.F.R. Pereira, Activated carbon catalytic ozonation of oxamic and oxalic acids, Appl. Catal. B: Environ. 79 (2008) 237–243.
[23] H.H. Huang, M.C. Lu, J.N. Chen, Catalytic decomposition of hydrogen peroxide and 4-chlorophenol in the presence of modified activated carbons, Chemosphere 51 (2003) 935–943.
[24] T.A. Kurniawan, W.H. Lo, Removal of refractory compounds from stabilized landfill leachate using an integrated H_2O_2 oxidation and granular activated carbon (GAC) adsorption treatment, Water Res. 43 (2009) 4079–4091.
[25] Z.Q. Liu, J. Ma, Y.H. Cui, B.P. Zhang, Effect of ozonation pretreatment on the surface properties and catalytic activity of multi-walled carbon nanotube, Appl. Catal. B: Environ. 92 (2009) 301–306.
[26] M. Sanchez-Polo, U. von Gunten, J. Rivera-Utrilla, Efficiency of activated carbon to transform ozone into ·OH radicals: Influence of operational parameters, Water Res. 39 (2005) 3189–3198.
[27] U. Jans, J. Hoigné, Activated carbon and carbon black catalyzed transformation of aqueous ozone into OH-radicals, Ozone-Sci. Eng. 20 (1998) 67–90.
[28] P.M. Álvarez, J.P. Pocostales, F.J. Beltrán, Granular activated carbon promoted ozonation of a food-processing secondary effluent, J. Hazard. Mater. 185 (2011) 776–783.
[29] T.A. Kurniawan, W.H. Lo, G.Y.S. Chan, Degradation of recalcitrant compounds from stabilized landfill leachate using a combination of ozone-GAC adsorption treatment, J. Hazard. Mater. B 137 (2006) 443–455.
[30] P.C.C. Faria, J.J.M. Orfão, Manuel Fernando R. Pereira, Mineralisation of coloured aqueous solutions by ozonation in the presence of activated carbon, Water Res. 39 (2005) 1461–1470.
[31] D.R. Grymonpré, W.C. Finney, B.R. Locke, Aqueous-phase pulsed streamer corona reactor using suspended activated carbon particles for phenol oxidation: model-data comparison, Chem. Eng. Sci. 54 (1999) 3095–3105.
[32] X.L. Hao, X.W. Zhang, L.C. Lei, Degradation characteristics of toxic contaminant with modified activated carbons in aqueous pulsed discharge plasma process, Carbon 47 (2009) 153–161.
[33] W.Z. Shen, H. Wang, R.G. Guan, Z.J. Li, Surface modification of activated carbon fiber and its adsorption for vitamin B1 and folic acid, Colloid Surf. A: Physicochem. Eng. Asp. 331 (2008) 263–267.
[34] S.J. Zhang, T. Shao, H.S. Kose, T. Karanfil, Adsorption of aromatic compounds by carbonaceous adsorbents: a comparative study on granular activated carbon, activated carbon fiber, and carbon nanotubes, Environ. Sci. Technol. 44 (2010) 6377–6383.
[35] M. Suzuki, Activated carbon fiber: fundamentals and applications, Carbon 32 (1994) 577–586.
[36] M. Carmo, M. Linardi, J.G.R. Poco, Characterization of nitric acid functionalized carbon black and its evaluation as electrocatalyst support for direct methanol fuel cell applications, Appl. Catal. A: Gen. 355 (2009) 132–138.
[37] P.M. Álvarez, J.F.G. Araya, F.J. Beltrán, F.J. Masa, F. Medina, Ozonation of activated carbons: effect on the adsorption of selected phenolic compounds from aqueous solutions, J. Colloid Interface Sci. 283 (2005) 503–512.
[38] H. Bader, J. Hoigne, Determination of ozone in water by the indigo method, Water Res. 15 (1981) 449–456.
[39] R.M. Selles, Spectrophotometric determination of hydrogen peroxide using potassium titanium (IV) oxalate, Analyst 105 (1980) 950–954.
[40] G.S. Vicente, A.R. Manuel, J. Antonio, Oxidation of activated carbon by hydrogen peroxide, study of surface functional groups by FTIR, Fuel 73 (1994) 387–395.
[41] C. Moreno-Castilla, M.V. López-Ramón, F. Carrasco-Marín, Changes in surface chemistry of activated carbons by wet oxidation, Carbon 38 (2000) 1995–2001.
[42] P.C.C. Faria, J.J.M. Órfão, M.F.R. Pereira, Ozone decomposition in water catalyzed by activated carbon: influence of chemical and textural properties, Ind. Eng. Chem. Res. 45 (2006) 2715–2721.
[43] K.D. Christopher, T.D. Waite, Process optimization of Fenton oxidation using kinetic modeling, Environ. Sci. Technol. 40 (2006) 4189–4195.
[44] J.A. Melero, G. Calleja, F. Martínez, R. Molina, M.I. Pariente, Nanocomposite Fe_2O_3/SBA-15: an efficient and stable catalyst for the catalytic wet peroxidation of phenolic aqueous solutions, Chem. Eng. J. 131 (2007) 245–256.
[45] L.A. Galeano, M.Á. Vicente, A. Gil, Treatment of municipal leachate of landfill by Fenton-like heterogeneous catalytic wet peroxide oxidation using an Al/Fe-pillared montmorillonite as active catalyst, Chem. Eng. J. 178 (2011) 146–153.
[46] A.L.T. Pham, C. Lee, F.M. Doyle, D.L. Sedlak, A silica-supported iron oxide catalyst capable of activating hydrogen peroxide at neutral pH, Environ. Sci. Technol. 43 (2009) 8930–8935.
[47] M.R. Ghezzar, F. Abdelmalek, M. Belhadj, N. Benderdouche, A. Addou, Gliding arc plasma assisted photocatalytic degradation of anthraquinonic acid green 25 in solution with TiO_2, Appl. Catal. B: Environ. 72 (2007) 304–313.
[48] J.Y. Gong, J. Wang, W.J. Xie, W.M. Cai, Enhanced degradation of aqueous methyl orange by contact glow discharge electrolysis using Fe^{2+} as catalyst, J. Appl. Electrochem. 38 (2008) 1749–1755.
[49] P. Lukes, A.T. Appleton, B.R. Locke, Hydrogen peroxide and ozone formation in hybrid gas–liquid electrical discharge reactors, IEEE Trans. Ind. Appl. 40 (2004) 60–67.
[50] M.R. Ghezzar, F. Abdelmalek, M. Belhadj, Enhancement of the bleaching and degradation of textile wastewaters by Gliding arc discharge plasma in the presence of TiO_2 catalyst, J. Hazard. Mater. 164 (2009) 1266–1274.
[51] J.B. Fernando, F.G.A. Juan, I. Giráldez, Gallic acid water ozonation using activated carbon, Appl. Catal. B: Environ. 63 (2006) 249–259.
[52] Q.S. Liu, T. Zheng, P. Wang, Adsorption isotherm, kinetic and mechanism studies of some substituted phenols on activated carbon fibers, Chem. Eng. J. 157 (2010) 348–356.
[53] J.P. Wang, H.M. Feng, H.Q. Yu, Analysis of adsorption characteristics of 2,4-dichlorophenol from aqueous solutions by activated carbon fiber, J. Hazard. Mater. 144 (2007) 200–207.
[54] M.F.R. Pereira, S.F. Soares, J.J.M. Orfao, J.L. Figueiredo, Adsorption of dyes on activated carbons: influence of surface chemical groups, Carbon 41 (2003) 811–821.
[55] L.R. Radovic, I.F. Silva, J.I. Ume, J.A. Menendez, C.A. Leon, Y. Leon, A.W. Scaroni, An experimental and theoretical study of the adsorption of aromatics possessing electron-withdrawing and electron-donating functional groups by chemically modified activated carbons, Carbon 35 (1997) 1339–1348.
[56] S.S. Barton, M.J.B. Evans, E. Halliop, J.A.F. MacDonald, Acidic and basic sites on the surface of porous carbon, Carbon 35 (1997) 1361–1366.
[57] J.A. Menendez, J. Phillips, B. Xia, L.R. Radovic, On the modification and characterization of chemical surface properties of activated carbon: In the search of carbons with stable basic properties, Langmuir 12 (1996) 4404–4410.
[58] J.H. Ramirez, F.J. Maldonado-Hódar, A.F. Pèrez-Cadenas, C. Moreno-Castilla, C.A. Costa, L.M. Madeira, Azo-dye Orange II degradation by heterogeneous Fenton-like reaction using carbon-Fe catalysts, Appl. Catal. B: Environ. 75 (2007) 312–323.
[59] A. Georgi, F.D. Kopinke, Interaction of adsorption and catalytic reactions in water decontamination processes. Part I. Oxidation of organic contaminants with hydrogen peroxide catalyzed by activated carbon, Appl. Catal. B: Environ. 58 (2005) 9–18.
[60] J. Rivera-Utrilla, M. Sanchez-Polo, Ozonation of naphthalenesulfphonic acid in aqueous phase in presence of basic activated carbons, Langmuir 20 (2004) 9217–9222.
[61] K.H. Barbara, Z. Maria, N. Jacek, Catalytic ozonation and methods of enhancing molecular ozone reactions in water treatment, Appl. Catal. B: Environ. 46 (2003) 639–669.